Chapter 8
Calcium-Induced Calcium Release

We started in Chap. 2 by assuming that the concentrations of the junctional sarcoplasmic reticulum (JSR) and the network sarcoplasmic reticulum (NSR) are identical and that the L-type current can be ignored and thus we studied a one-dimensional problem where the calcium concentration of the dyad was the only variable of interest. The model is illustrated in Figs. 2.1 and 2.2. Then, in Chap. 5, we extended the model to account for the varying concentrations in the dyad and the JSR, but we still ignored the effect of the voltage-gated L-type channels and kept the concentration of the cytosol and the NSR constant. The two-dimensional model is illustrated in Figs. 5.1 and 5.2. Our aim is now to include the effect of L-type channels. The L-type channels open and close depending on the transmembrane potential V, so the model will therefore be parameterized by V. The model is illustrated in Figs. 8.1 and 8.2.

It should be noted that we are still interested in the dynamics related to the dyad and not to the whole cell. We therefore keep the concentration of the cytosol and NSR constant and assume that the concentration of the extracellular space (c_e) only affects the concentration of the dyad through the voltage-gated L-type calcium channels (LCCs). In a whole-cell model, this would be different in many ways, but we shall not consider that topic here.

The state of a voltage-gated channel is governed by a Markov model where the transitions depend on the transmembrane potential (or voltage for short). If the electrical potential in the dyad is given by V_i (intracellular potential) and the extracellular potential is given by V_e, we define the transmembrane potential to be

$$V = V_i - V_e.$$

As a notational convention, we use the subscript r to indicate that $\bar{\gamma}_r$ models the open or closed state of the ryanodine receptor (RyR) and the subscript l in the term $\bar{\gamma}_l J_l$ is used to indicate that this is the flux through the LCC.
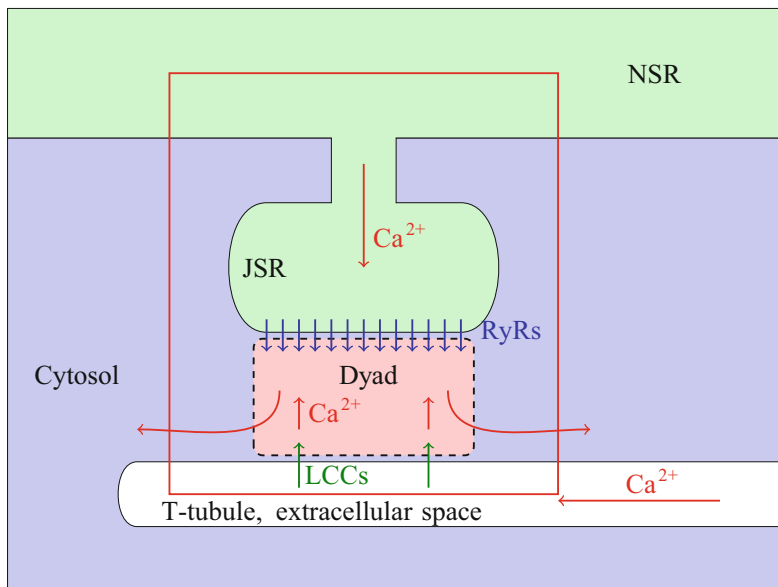
Fig. 8.1 The figure is a modified version of Figure 1 (panel A) of Winslow et al. [105] and illustrates the components involved in calcium-induced calcium release (CICR). In this chapter, we concentrate on the dynamics in the box surrounded by a *thin red line*. We assume that the concentrations of the cytosol, the NSR, and the extracellular domain represented by the T-tubule are kept constant and that inflow of calcium through the LCCs is governed by a voltage-dependent Markov model

	Extracellular, c_e		
Cytosol, c_0	Dyad, $\bar{x}(t)$	JSR, $\bar{y}(t)$	NSR, c_1

Fig. 8.2 Sketch of a release unit. The cytosolic (c_0), NSR (c_1), and extracellular (c_e) calcium concentrations are assumed to be constant, while the concentrations of the dyad and JSR are given by $\bar{x} = \bar{x}(t)$ and $\bar{y} = \bar{y}(t)$, respectively. Furthermore, we assume that the flux of calcium from the extracellular space to the dyad is voltage gated. Recall that $c_0 \ll c_1$

8.1 Stochastic Release Model Parameterized by the Transmembrane Potential

In the models we have studied so far, a very basic building block has been that, if x_0 denotes the concentration of a large reservoir of calcium and $x = x(t)$ denotes the concentration of a small space connected to the reservoir, then the concentration x

Table 8.1 Values of parameters used in simulations in this chapter

v_d	1 ms^{-1}
v_r	0.1 ms^{-1}
v_s	0.01 ms^{-1}
c_0	0.1 μM
c_1	1,000 μM
c_e	1,800 μM

evolves according to the model

$$x'(t) = v\,(x_0 - x(t)),\tag{8.1}$$

where v denotes the speed of diffusion between the two spaces. Here we assume that the concentration of the large reservoir, x_0, can be kept constant. This model can be extended to the case where the channel between the spaces can be either closed or open:

$$\bar{x}'(t) = \bar{\gamma}(t)v\,(x_0 - \bar{x}(t)),\tag{8.2}$$

where $\bar{\gamma}$ is a random variable taking on two possible values, one (open) and zero (closed). The stochastic release models studied above are derived by gluing together pieces of models of exactly this type.

In this chapter, one additional effect is added: We now allow calcium to flow into the dyad through the LCCs. This flow depends on both the gradient of the concentration and of the electrical potential across the membrane dividing the extracellular space and the dyad.

The process illustrated in Fig. 8.2 can be modeled as follows

$$\bar{x}' = \bar{\gamma}_r v_r\,(\bar{y} - \bar{x}) + v_d\,(c_0 - \bar{x}) - \bar{\gamma}_l J_l,\tag{8.3}$$

$$\bar{y}' = \bar{\gamma}_r v_r\,(\bar{x} - \bar{y}) + v_s\,(c_1 - \bar{y}).\tag{8.4}$$

This model is almost the same as the one we analyzed above (see (5.1) and (5.2) on page 92). The new term is given by $-\bar{\gamma}_l J_l$ and it models the inflow of calcium through the LCCs. The function $\bar{\gamma}_l$ is governed by a Markov model and, as usual, it takes on two values: zero (closed) and one (open). The Markov model governing $\bar{\gamma}_l$ depends on the transmembrane potential V and the flux depends on V, the extracellular calcium concentration c_e and the dyad concentration $x = x(t)$. As above, v_r denotes the rate of release from the JSR to the dyad, v_d denotes the speed of calcium diffusion from the dyad to the cytosol, and v_s denotes the speed of calcium diffusion from the NSR to the JSR. The model parameters are given in Table 8.1.

The Markov model governing $\bar{\gamma}_r$ will be the same as above, but we need to introduce a Markov model governing $\bar{\gamma}_l$. We will also combine these Markov models to simplify the introduction of a probability density formulation. Furthermore, we need to describe the electrochemical flux J_l.

8.1.1 Electrochemical Goldman–Hodgkin–Katz (GHK) Flux

Consider Fig. 8.1 and suppose that the membrane between the T-tubule and the dyad has thickness L. If the electrical field is constant through the channel, the flux is given by

$$J_l = \frac{D}{L} \frac{2F}{RT} \frac{x - c_e e^{-\frac{2FV}{RT}}}{1 - e^{-\frac{2FV}{RT}}} V, \tag{8.5}$$

which is referred to as the GHK flux (see Keener and Sneyd [42]). Here D is Fick's diffusion constant, F is Faraday's constant, R is the gas constant, and T is the absolute temperature. By defining

$$V_0 = \frac{RT}{2F},$$

we have

$$J_l = \frac{D}{L} \frac{x - c_e e^{-\frac{V}{V_0}}}{1 - e^{-\frac{V}{V_0}}} \frac{V}{V_0}, \tag{8.6}$$

where F, R, T, and V_0 are given in Table 8.2.

8.1.2 Assumptions

As for the model in Chap. 5, we will make the following assumptions for the parameters involved:

$$c_1 \gg c_0 \quad \text{and} \quad v_r, v_d, v_s > 0, \tag{8.7}$$

$$v_d v_s \geq v_r^2. \tag{8.8}$$

Table 8.2 Parameters in (8.5)

F	96485.3 C mol^{-1}
R	8.3145 J mol^{-1}K^{-1}
T	310 K
V_0	13.357 mV
$\frac{D}{L}$	0.02 ms^{-1}

8.1.3 Equilibrium Potential

The electrochemical equilibrium over the membrane separating the extracellular space and the dyad is characterized by

$$J_l = 0.$$

In equilibrium, we must have

$$x = c_e e^{-\frac{V}{V_0}},$$

so the equilibrium transmembrane potential is given by

$$V_{eq} = V_0 \ln \frac{c_e}{x}. \tag{8.9}$$

For this value of the transmembrane potential V, the driving force $-\bar{\gamma}_l J_l$ in the system (8.3) and (8.4) is zero even if the channel is open. It should also be noted that the equilibrium transmembrane potential depends on the concentration x of the dyad and will therefore be a dynamic quantity. Here it is useful to recall that we regard V as a parameter input to the system and not a part of the dynamics.

8.1.4 Linear Version of the Flux

We mentioned above that our modeling so far has been based on very simple linear fluxes of the form given in (8.1). In the case we are considering now, the flux depends on both the difference in concentration and the electrical potential over the membrane; see (8.6). A Taylor series expansion of the GHK flux can be written as

$$J_l = \frac{D}{L}(x - c_e) + \frac{D}{2L}(x + c_e)\frac{V}{V_0} + O\left((V/V_0)^2\right) \tag{8.10}$$

and, therefore, if $V = 0$, the flux is given by

$$J_l = \frac{D}{L}(x - c_e)$$

so the term $-\bar{\gamma}_l J_l$ has the form we used in (8.2). This means that the electrochemical flux given by (8.6) reduces to a purely concentration-based flux when there is no difference in electrical potential across the membrane.

8.1.5   Markov Models for CICR

As discussed above, two Markov processes are involved in the CICR. We have seen
that the gating of the release of calcium from the sarcoplasmic reticulum to the dyad
is given by the stochastic variable $\bar{\gamma}_r = \bar{\gamma}_r(t)$, which is governed by the reaction
scheme

$$C_r \underset{k_{co}^r}{\overset{k_{oc}^r}{\rightleftarrows}} O_r. \tag{8.11}$$

We recall here that r is used to indicate the relation to the RyR channels. Similarly,
the Markov model for the LCC is given by

$$C_l \underset{k_{co}^l}{\overset{k_{oc}^l}{\rightleftarrows}} O_l, \tag{8.12}$$

where l is used to indicate the relation to the LCCs. This Markov model governs the
stochastic variable $\bar{\gamma}_l = \bar{\gamma}_l(t)$.

It is convenient to combine these two Markov models into one reaction scheme of
the form illustrated in Fig. 8.3. The states of this combined Markov model are given
by C_lC_r (both closed), C_lO_r (LCC closed, RyR open), O_lO_r (both open), and O_lC_r
(LCC open, RyR closed). In our computations, we use the rates shown in Table 8.3.

Fig. 8.3   Markov model
including four possible states:
C_lC_r (both closed), C_lO_r
(LCC closed, RyR open),
O_lO_r (both open), and O_lC_r
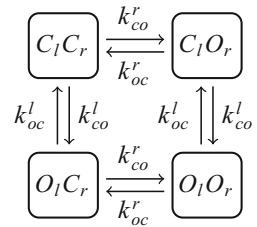(LCC open, RyR closed)

Table 8.3   Reaction rates used in the Markov model illustrated in Fig. 8.3. Here $\mu \geq 1$ denotes
the mutation severity index of the RyR, $\eta \geq 1$ denotes the mutation severity index of the LCC and
$\mu = \nu = 1$ represents the wild type case

RyR	LCC
$k_{co}^r = \mu \frac{x^4}{K(y)^4 + x^4}$ ms^{-1}	$k_{co}^l = \eta\, l_\infty(V)/\tau_l$
$k_{oc}^r = 1$ ms^{-1}	$k_{oc}^l = (1 - l_\infty(V))/\tau_l$
$K(y) = K_{max} - y/1000$	$l_\infty(V) = 0.01 \exp(-(V-5)^2/500)$
$K_{max} = 7.4\ \mu$M	$\tau_l = 1$ ms

8.1.6   Numerical Scheme for the Stochastic CICR Model

A numerical scheme for running simulations based on the CICR model (8.3) and (8.4) is given by

$$x_{n+1} = x_n + \Delta t \left(\gamma_n^r v_r \left(y_n - x_n \right) + v_d \left(c_0 - x_n \right) \right) - \Delta t \gamma_n^l J_l(x_n, V), \qquad (8.13)$$

$$y_{n+1} = y_n + \Delta t \left(\gamma_n^r v_r \left(x_n - y_n \right) + v_s \left(c_1 - y_n \right) \right), \qquad (8.14)$$

where γ_n^r and γ_n^l are computed according to the Markov model illustrated in Fig. 8.3.

8.1.7   Monte Carlo Simulations of CICR

In Fig. 8.4, we show the results of stochastic simulations using the model (8.3) and (8.4). The computations are based on the numerical scheme (8.13) and (8.14) with the parameters given in Table 8.1 and $\Delta t = 0.01$ ms. As initial conditions we have used $x(0) = c_0$ and $y(0) = c_1$ with both gates closed. From top to bottom, the transmembrane potential is given by $V = 20, 0, -20$, and -40 mV.

The associated calcium concentrations of the dyad given by $x = x(t)$ are graphed in the left panels and the calcium concentrations of the JSR given by $y = y(t)$ are graphed in the right panels. In all cases, we show the solution for a time interval ranging from 0 ms to 1000 ms. The calcium concentration clearly depends on the transmembrane potential and we observe in particular that there is no activity for $V = -40$ mV, since the LCC is inactivated at that voltage.

In Fig. 8.5, we show a detailed view of the case of $V = 0$ mV. In the upper part of the graph we show the state of the RyR (upper) and the LCCs (lower). The CICR mechanism is illustrated in the first part of the graph: The LCC opens at $t \approx 5$ ms, but the release is too short-lived to trigger an RyR opening and we therefore observe just a minor increase in the dyad calcium concentration given by x. Next time, at $t \approx 9$ ms, there is a new opening and now the channel is open for a longer time; there is an increase in x leading to opening of the RyR channel and then the concentration increases dramatically.

8.2   Invariant Region for the CICR Model

We have seen in both the one- and two-dimensional models above that we can derive invariant regions for the stochastic models and that these regions define the computational domain for the probability density system. Our aim is now to derive
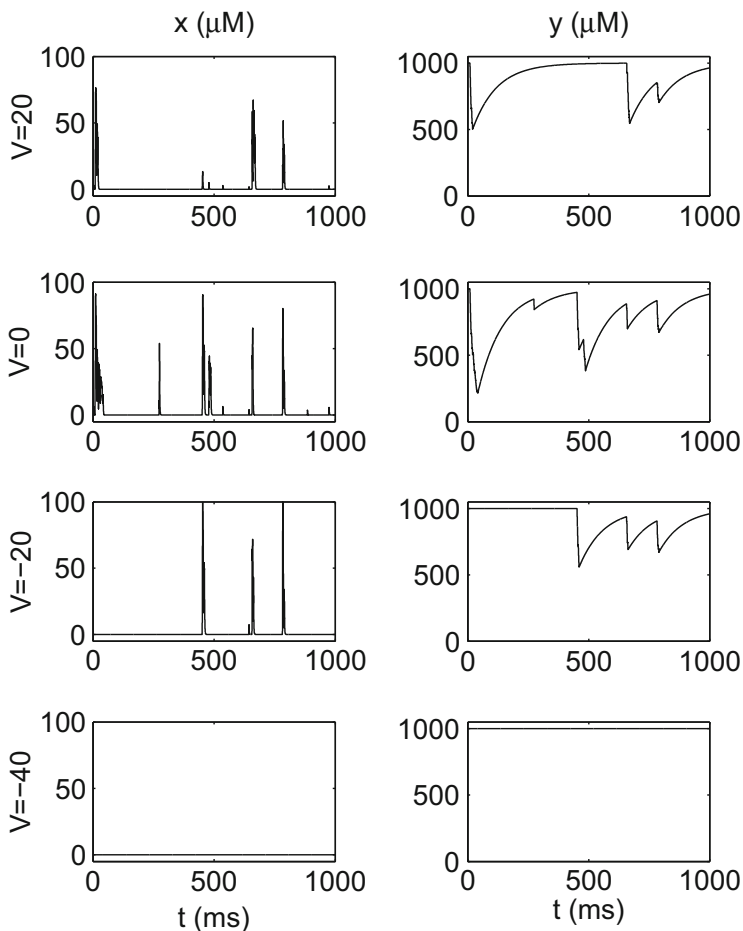
Fig. 8.4 Calcium dynamics of the dyad $x = x(t)$ and the JSR $y = y(t)$ for four values of the transmembrane potential V

an invariant region for the CICR model given by

$$\bar{x}' = \bar{\gamma}_r v_r \left(\bar{y} - \bar{x}\right) + v_d \left(c_0 - \bar{x}\right) - \bar{\gamma}_l J_l, \tag{8.15}$$

$$\bar{y}' = \bar{\gamma}_r v_r \left(\bar{x} - \bar{y}\right) + v_s \left(c_1 - \bar{y}\right). \tag{8.16}$$

Here it is convenient to write the GHK flux in the form

$$J_l(x) = a_0(x - x_0),$$
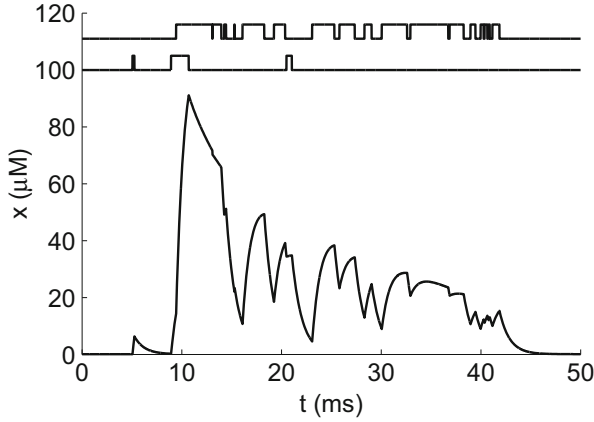
Fig. 8.5 A detailed view of the case of $V = 0$ mV taken from Fig. 8.4. In addition, we show the state of the RyR channel (*upper panel*) and the LCC (*lower panel*). The first spike at 5 ms in the LCC is very short and does not trigger an RyR release. The next one, at 9 ms, does trigger an RyR release

where

$$a_0 = \frac{D}{L} \frac{1}{1 - e^{-\frac{V}{V_0}}} \frac{V}{V_0}$$

and

$$x_0 = c_e e^{-\frac{V}{V_0}},$$

so the system takes the form

$$\bar{x}' = \bar{\gamma}_r v_r (\bar{y} - \bar{x}) + v_d (c_0 - \bar{x}) + \bar{\gamma}_l a_0 (x_0 - \bar{x}), \qquad (8.17)$$

$$\bar{y}' = \bar{\gamma}_r v_r (\bar{x} - \bar{y}) + v_s (c_1 - \bar{y}) . \qquad (8.18)$$

8.2.1 A Numerical Scheme

Let us consider the numerical scheme (8.13, 8.14),

$$x_{n+1} = x_n + \Delta t \left(\gamma_n^r v_r (y - x) + v_d (c_0 - x) + \gamma_n^l a_0 (x_0 - x) \right), \qquad (8.19)$$

$$y_{n+1} = y_n + \Delta t \left(\gamma_n^r v_r (x - y) + v_s (c_1 - y) \right). \qquad (8.20)$$

Here γ_n^r and γ_n^l simply denotes constants that take on the value zero or one and their values will be specified in order to study the dynamics of the system when the

associated channels are open or closed. The numerical scheme can be written in the
form

$$x_{n+1} = F(x_n, y_n),\tag{8.21}$$

$$y_{n+1} = G(x_n, y_n),\tag{8.22}$$

with

$$F(x, y) = x + \Delta t \left(\gamma_r v_r (y - x) + v_d (c_0 - x) + \gamma_l a_0 (x_0 - x) \right),$$

$$G(x, y) = y + \Delta t \left(\gamma_r v_r (x - y) + v_s (c_1 - y) \right).$$

Here we assume that

$$\Delta t \leqslant \min \left(\frac{1}{v_d + a_0 + v_r}, \frac{1}{v_s + v_r} \right).\tag{8.23}$$

Under this condition, we observe that

$$\frac{\partial F}{\partial x} = 1 - \Delta t \left(v_d + \gamma_l a_0 + \gamma_r v_r \right) \geqslant 0$$

for any choice of γ_l and γ_r. We also have

$$\frac{\partial F}{\partial y} = \Delta t \gamma_r v_r \geqslant 0.$$

Similarly, we find that

$$\frac{\partial G}{\partial x} = \Delta t \gamma_r v_r \geqslant 0\tag{8.24}$$

and

$$\frac{\partial G}{\partial y} = 1 - \Delta t \left(v_s + \gamma_r v_r \right) \geqslant 0.\tag{8.25}$$

Assume that

$$0 \leqslant x_n, y_n \leqslant M,\tag{8.26}$$

where

$$M = \max \left(c_1, \frac{c_0 v_d + a_0 x_0}{a_0 + v_d} \right).$$

Since

$$\frac{\partial F}{\partial x}, \frac{\partial F}{\partial y}, \frac{\partial G}{\partial x}, \frac{\partial G}{\partial y} \geqslant 0,$$

we have

$$x_{n+1} = F(x_n, y_n) \leqslant F(M, M) = M + \Delta t (v_d (c_0 - M) + \gamma_l a_0 (x_0 - M)) \leqslant M$$

and

$$y_{n+1} = G(x_n, y_n) \leqslant G(M, M) = M + \Delta t (v_s (c_1 - M)) \leqslant M.$$

Furthermore, we have

$$x_{n+1} = F(x_n, y_n) \geqslant F(0, 0) = \Delta t (v_d c_0 + \gamma_l a_0 x_0) \geqslant 0$$

and

$$y_{n+1} = G(x_n, y_n) \geqslant G(0, 0) = \Delta t v_s c_1 \geqslant 0.$$

So, by induction, the invariant region (8.26) holds for all $n \geqslant 0$.

8.3 Probability Density Model Parameterized by the Transmembrane Potential

The probability density formulation of the system (8.3) and (8.4) is given by the system of partial differential equations

$$\frac{\partial \rho_{oo}}{\partial t} + \frac{\partial}{\partial x} \left(a_{oo}^x \rho_{oo} \right) + \frac{\partial}{\partial y} \left(a_{oo}^y \rho_{oo} \right) = k_{co}^l \rho_{co} - \left(k_{oc}^l + k_{oc}^r \right) \rho_{oo} + k_{co}^r \rho_{oc}, \quad (8.27)$$

$$\frac{\partial \rho_{oc}}{\partial t} + \frac{\partial}{\partial x} \left(a_{oc}^x \rho_{oc} \right) + \frac{\partial}{\partial y} \left(a_{oc}^y \rho_{oc} \right) = k_{co}^l \rho_{cc} - \left(k_{oc}^l + k_{co}^r \right) \rho_{oc} + k_{oc}^r \rho_{oo}, \quad (8.28)$$

$$\frac{\partial \rho_{cc}}{\partial t} + \frac{\partial}{\partial x} \left(a_{cc}^x \rho_{cc} \right) + \frac{\partial}{\partial y} \left(a_{cc}^y \rho_{cc} \right) = k_{oc}^l \rho_{oc} - \left(k_{co}^l + k_{co}^r \right) \rho_{cc} + k_{oc}^r \rho_{co}, \quad (8.29)$$

$$\frac{\partial \rho_{co}}{\partial t} + \frac{\partial}{\partial x} \left(a_{co}^x \rho_{co} \right) + \frac{\partial}{\partial y} \left(a_{co}^y \rho_{co} \right) = k_{oc}^l \rho_{oo} - \left(k_{co}^l + k_{oc}^r \right) \rho_{oc} + k_{co}^r \rho_{cc}, \quad (8.30)$$

where $\rho_{oo}, \rho_{oc}, \rho_{cc}$, and ρ_{co} represent the probability densities of the states denoted O_lO_r, O_lC_r, C_lC_r, and C_lO_r, respectively. The terms of the fluxes are given by

$$
\begin{aligned}
a_{oo}^x &= v_r \, (y - x) + v_d \, (c_0 - x) - J_l(x, V), & a_{oo}^y &= v_r \, (x - y) + v_s \, (c_1 - y), \\
a_{oc}^x &= v_d \, (c_0 - x) - J_l(x, V), & a_{oc}^y &= v_s \, (c_1 - y), \\
a_{cc}^x &= v_d \, (c_0 - x), & a_{cc}^y &= v_s \, (c_1 - y), \\
a_{co}^x &= v_r \, (y - x) + v_d \, (c_0 - x), & a_{co}^y &= v_r \, (x - y) + v_s \, (c_1 - y),
\end{aligned}
$$

where we use the convention that in the expression $a_{\alpha\beta}^x$, the index α indicates whether the LCC is open ($\alpha = o$) or closed ($\alpha = c$) and the index β plays the same role for the RyR channel. Similar notation is used for the flux terms represented by $a_{\alpha\beta}^y$. As usual, the sum of total probabilities is one:

$$
\int_\Omega (\rho_{oo} + \rho_{oc} + \rho_{cc} + \rho_{co}) \, dx \, dy = 1. \tag{8.31}
$$

8.4   Computing Probability Density Representations of CICR

In Fig. 8.6, we show solutions of the system (8.15) and (8.16) defined in the computational domain $\Omega = \Omega(V)$ for four values of the transmembrane potential: $V = 20, 0, -20$, and -40 mV. In all computations, the parameters are given in Table 8.1 and the Markov model is illustrated in Fig. 8.3. All distributions are initially set to zero, except that $\rho_{cc}(c_0, c_1) = 1/(\Delta x \Delta y)$. Hence the initial discrete probability densities integrates to one;

$$
\Delta x \Delta y \sum_{i,j} \rho_{i,j} = 1, \tag{8.32}
$$

which is a discrete version of (8.31) with $\rho = \rho_{oo} + \rho_{oc} + \rho_{co} + \rho_{cc}$.

The simulation results are shown in Fig. 8.6 and summarized in Table 8.4. We observe that the transmembrane potential V significantly influences the probability density functions. In Table 8.4, we observe that the probability of the LCC being in the open state is highest for $V = 0$ mV and it is almost zero for $V = -40$ mV. In the computations, we use $\Delta t = 0.001$ ms, $\Delta x = 1.02, 1.23, 1.54$ and $1.95\ \mu$M (the domain size varies with V), and $\Delta y = 9.3\ \mu$M. Note that the scale of the plots varies (see Fig. 8.6).
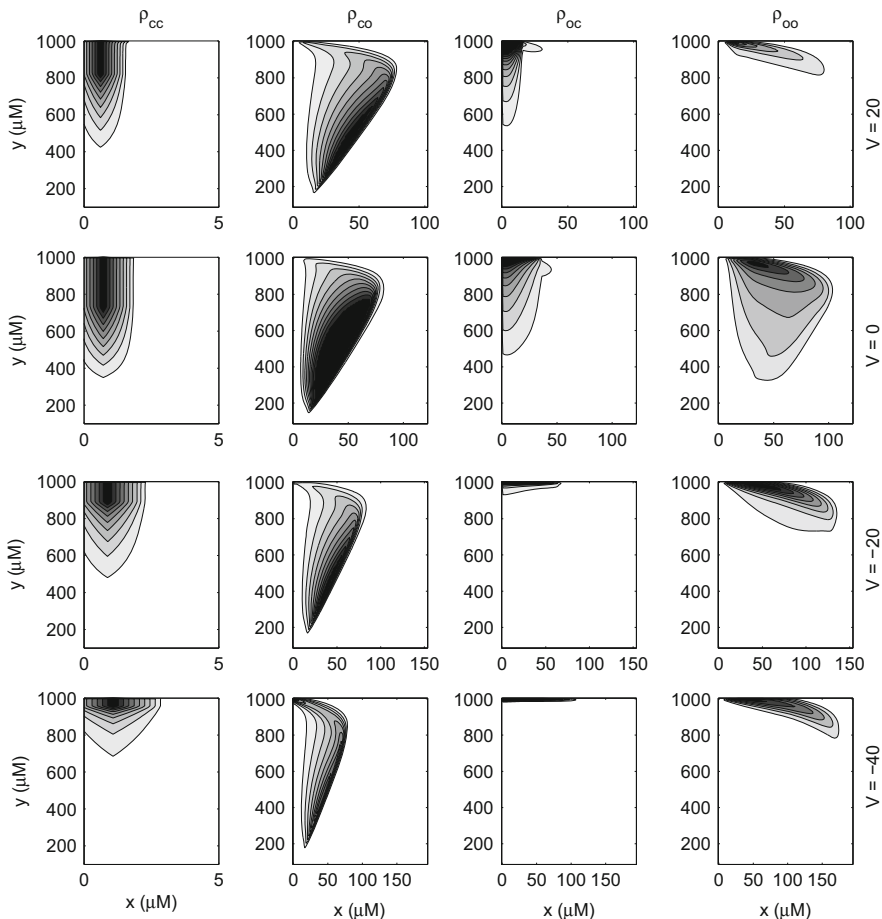
Fig. 8.6 Probability density functions for different voltages. The LCC is more prone to being open (last two columns) when the voltage is close to $V = 5$ mV, that is, where $l_\infty(V)$ is close to its maximum. Black corresponds to 10^{-3} for ρ_{cc} and to 10^{-6} for the other three distributions

Table 8.4 Probability of being in the four states for different voltages. Recall that the probabilities are computed using (4.7) at page 72 where the probability density functions are numerical solutions of the system (8.27)–(8.30)

V	π_{cc}	π_{co}	π_{oc}	π_{oo}
20	0.978	0.015	0.005	0.001
0	0.959	0.032	0.007	0.003
−20	0.982	0.015	0.002	0.001
−40	0.993	0.006	0.000	0.000

8.5 Effects of LCC and RyR Mutations

We are now in a position to study the effect of both LCC and RyR mutations. We assume that both the LCC and RyR mutations lead to leaky channels that can be represented by increasing the reaction rate from closed to open. So we again consider CO-mutations.

The reaction scheme in the presence of mutations is illustrated in Fig. 8.7. Here $\mu \geq 1$ denotes the strength of the RyR mutations and $\eta \geq 1$ denotes the strength of the LCC mutations. Note that $\mu = 1$ and $\eta = 1$ represent the wild type.

8.5.1 Effect of Mutations Measured in a Norm

To measure the effect of the mutations, we introduce the norm

$$\|\rho^{\eta,\mu} - \rho^{1,1}\| = \frac{1}{6} \sum_{V} \sum_{z} \frac{\|\rho_z^{\eta,\mu} - \rho_z^{1,1}\|_{L^2(\Omega)}}{\|\rho_z^{\eta,\mu}\|_{L^2(\Omega)} + \|\rho_z^{1,1}\|_{L^2(\Omega)},} \tag{8.33}$$

where ρ_z represents $\rho_{oo}, \rho_{oc}, \rho_{co}$, or ρ_{cc} and V represents summation over the following values of the transmembrane potential: $-80, -60, -40, -20, 0$, and 20 mV. Furthermore,

$$\|\rho\|_{L^2(\Omega)} = \left(\int_{\Omega} \rho^2 d\Omega \right)^{1/2}. \tag{8.34}$$

The difference between the wild type solution and the solution based on mutated reaction rates is depicted in Fig. 8.8. The figure shows the difference as a function of the two mutation severity indices μ and η.

Fig. 8.7 Mutant version of the Markov model given in Fig. 8.3 including four possible states: $C_l C_r$ (both closed), $C_l O_r$ (LCC closed, RyR open), $O_l O_r$ (both open), and $O_l C_r$ (LCC open, RyR closed)
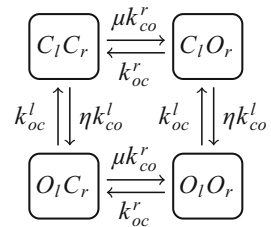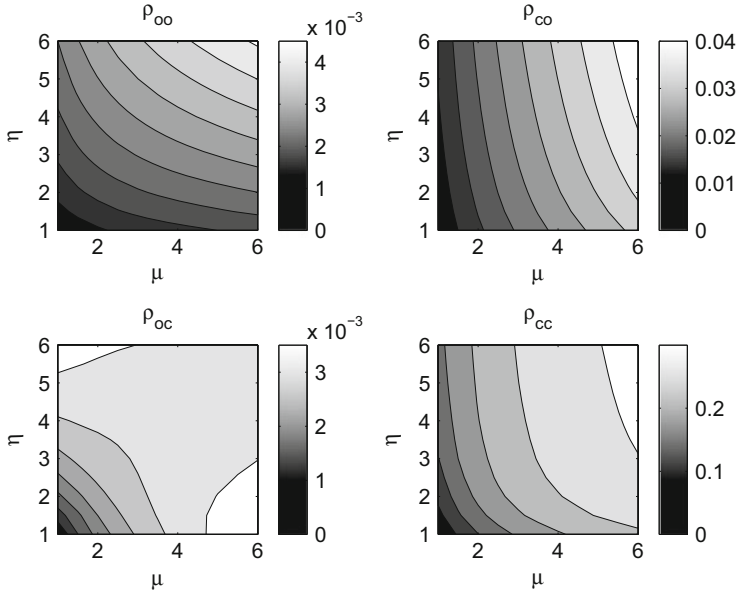
Fig. 8.8 Difference between wild type solutions and mutated solutions, defined in terms of the norm given by (8.33). The wild type solution is represented by $\mu = \eta = 1$

8.5.2   Mutations Increase the Open Probability of Both the LCC and RyR Channels

In Sect. 4.2 (page 72), we introduced statistical measures for the probability density functions. We will now consider how the LCC and RyR mutations affect the statistical properties of the associated probability density functions. Let us first consider how the mutations affect the total probability of being in the different states. In Fig. 8.9, we show the total probability of being in the states OO, CO, OC, and CC, where, as above, the first letter denotes the state of the LCC and the second letter indicates the state of the RyR channel. Here the value of the transmembrane potential is $V = 0$ mV. In Fig. 8.10, we show similar results in the case of $V = -80$ mV; the probability of the LCC being open is very small and the LCC mutation must be extremely severe to change this. Basically, at $V = -80$ mV, the LCC is closed independent of the mutations. This observation certainly depends heavily on the particular reaction rates used in these computations (see Table 8.3 on page 130).
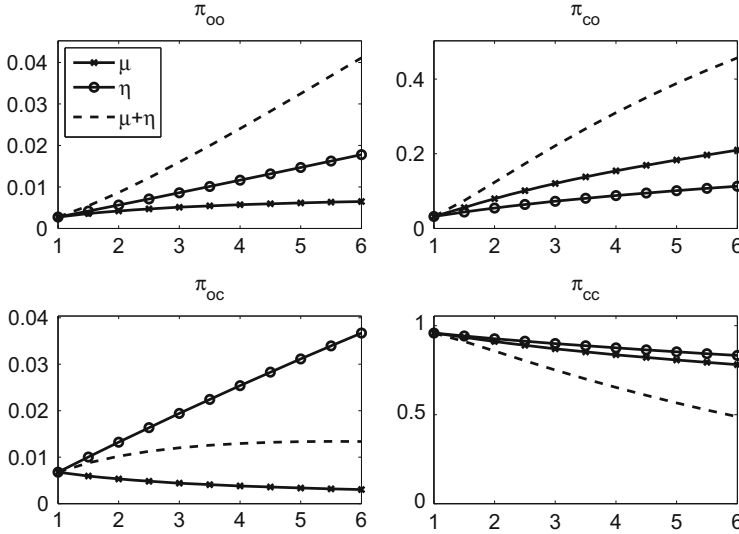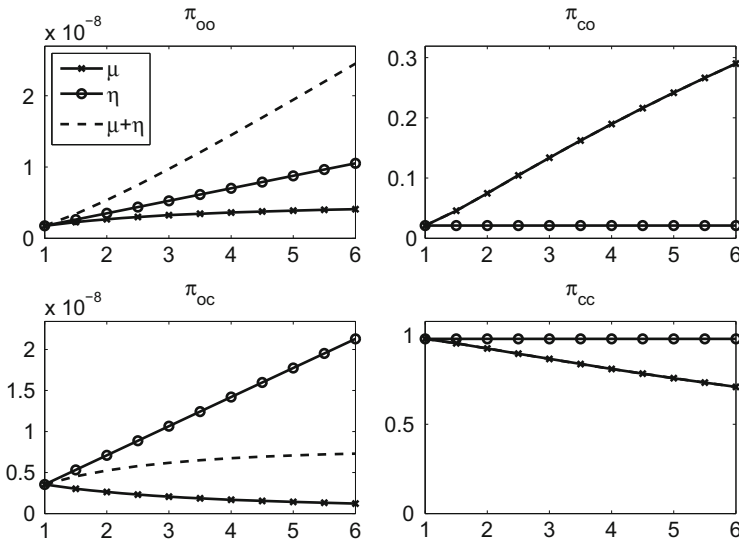
Fig. 8.9 Probability of being in the state OO, CO, OC, or CC at $V = 0$ mV as a function of the mutation severity index of the LCC, represented by η, and the mutation severity index of the RyR channel, represented by μ. Here $\eta = \mu = 1$ represents the wild type

Fig. 8.10 Probability of being in the state OO, CO, OC, or CC at $V = -80$ mV as a function of the mutation severity index of the LCC, represented by η, and the mutation severity index of the RyR channel, represented by μ. Here $\eta = \mu = 1$ represents the wild type. Note the scale of the axis in the plots on the left-hand side

8.5.3   Mutations Change the Expected Values of Concentrations

Figures 8.11 and 8.12 show the development of the expected concentration for varying strengths of mutations. In Fig. 8.11, we set $V = 0$ mV and see that the mutations change the expected concentrations significantly. More specifically, both mutations lead to lower expected JSR concentrations. In Fig. 8.12, we set $V = -80$ mV and observe that the expected concentrations are not altered by the LCC mutation. As for the total probabilities discussed above, the reason for this is that, at this value of V, the probability of going from closed to open is practically zero and the mutation must be orders of magnitude larger to open the LCC at this voltage. Again, this observation is based on the particular form of the reaction rates given in Table 8.3.
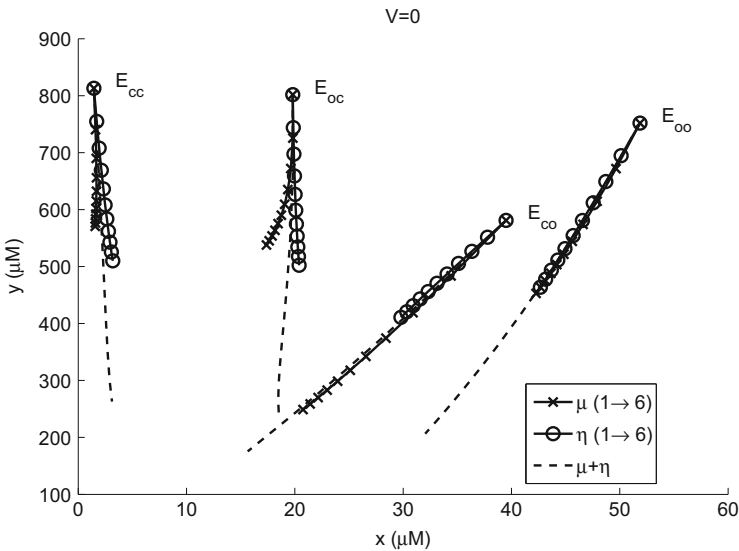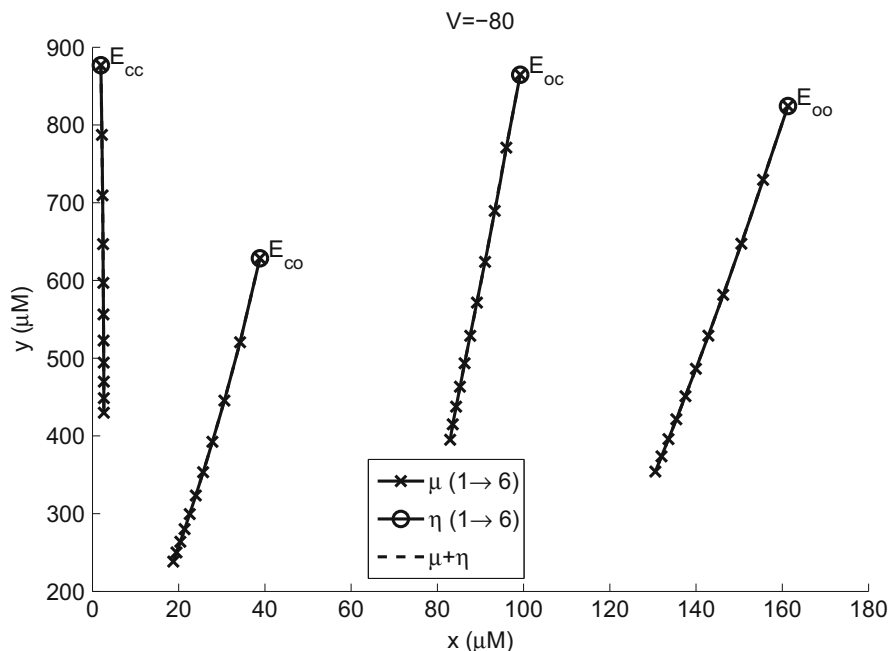

Fig. 8.11 This figure shows how the expected concentrations of the dyad (given by x) and the JSR (given by y) change as functions of the mutation severity indices. The curve denoted by E_{cc} starts at the circle that represents the expected values of x and y in the case of both the LCC and RyR being closed. The starting point represents the wild type and the curves represent the two mutations (or combinations of them) and similarly for the curves starting at the circles next to E_{oc}, E_{co}, and E_{oo}. All curves are computed using $V = 0$ mV

Fig. 8.12 This figure shows how the expected concentrations of the dyad (given by x) and the JSR (given by y) change as functions of the mutation severity indices. The curve denoted by E_{cc} starts at the circle that represents the expected values of x and y in the case of both LCC and RyR being closed. The starting point represents the wild type and the curves represent the two mutations (or combinations of them) and similarly for the curves starting at the circles next to E_{oc}, E_{co}, and E_{oo}. All curves are computed using $V = -80$ mV

8.6   Notes

1. The Markov model (including parameters) given in Fig. 8.3 and the probability density system (8.27)–(8.30) are taken from Williams et al. [102].
2. The functions given in Table 8.3 are motivated by the models of Stern et al. [89].